Check for updates

Statistical analysis of apparent morphology and characteristics of corroded rebars of concrete in the marine environment

Zongquan Ying[1,2,3,4]*, Jiamin Li[1,2,3,4] and Juan Zhao[1,2,3,4]

[1]CCCC Fourth Harbor Engineering Institute Co., Ltd., Guangzhou, China, [2]Key Laboratory of Hydraulic Structure Durability Technology for Transportation Industry, Guangzhou, China, [3]Key Laboratory of Construction Material, CCCC, Guangzhou, China, [4]Observation and Research Base of Transport Industry of Long-term Performances of Marine Infrastructure, Ministry of Transport, Guangzhou, China

The residual cross-sectional areas of corroded rebars and their uniformity are the main indexes to evaluate the safety and durability of concrete structures in the marine environment. To evaluate corrosion characteristics of naturally corroded rebars, nineteen corroded rebars were extracted from the prototype components of a high-pile wharf with 35 years of service. The apparent morphology characteristics of corroded rebars were obtained using 3D scanning. The results indicate that the corrosion is non-uniform along both the longitudinal and cross-sectional directions of the corroded rebars. In the marine environment, the residual cross-sectional areas of corroded rebars along the length adhere to a three-parameter Weibull distribution; however, no specific probability distribution model or clear correlation with the distribution pattern exists for rebars with varying corrosion degrees. The spatial heterogeneity factors of the rebars are characterized by a three-parameter Frechet distribution.

Highlights

- Rebars have been corroded in the marine environment for 35 years.
- The corrosion is non-uniform along the length direction and cross-section direction of rebars.
- The residual cross-sectional areas follow a three-parameter Weibull distribution.
- The spatial heterogeneity factors obey a three-parameter Frechet distribution.

1 Introduction

Reinforcement corrosion is one of the main factors leading to the degradation of durability (Bazant, 1979; Costa and Appleton, 2002) and a decline in the bearing capacity (Bhargava et al., 2007; Xia et al., 2016) of reinforced concrete members. To quantitatively evaluate the influence of the degree of steel corrosion on the bearing capacity of components, numerous scholars have investigated its impact on mechanical properties (Du et al., 2005; Zhang et al., 2012; Francois et al., 2013). However, these studies did not

account for the non-uniform corrosion of rebars, and instead used the average corrosion rate of rebars (average mass loss or average cross-sectional area loss) to describe the degree of corrosion. Studies (Almusallam, 2001; Maslehuddin et al., 1990) have found that for non-uniform corrosion, the nominal tensile strength of corroded rebar is significantly lower than that of uncorroded rebar. Moreover, the elongation of corroded rebar decreases obviously with increasing corrosion degree, and tends to brittle failure gradually. Apostolopoulos et al. (2013) observed that compared with uniform corrosion, pitting corrosion led to significantly greater plastic degradation of rebars. Furthermore, non-uniform corrosion of reinforcement may induce failure in non-critical section of components, with the failure probability of reinforced concrete beams increasing by 200% under non-uniform corrosion condition (Stewart and Al-Harthy, 2008).

Chloride ion erosion causes the corrosion of rebars in concrete structures to be both uneven and time-dependent. Due to the uneven external environment and material properties, the apparent morphology of corroded rebar exhibits significant randomness and complexity. Currently, the primary methods for measuring the corrosion rate and apparent morphological characteristics of corroded rebars include the weighing method (Yi et al., 2010; Zhang et al., 2010; Malumbela et al., 2010; Zhu et al., 2013), vernier caliper method (Torres-Acosta and Castro-Borges, 2013), drainage method (Du et al., 2005), X-ray imaging method (Xi and Yang, 2019), CT imaging method (Lim et al., 2017; Fernandez et al., 2018) and 3D scanning method (Kashani et al., 2013; Zhang J. Z. et al., 2021; Tang et al., 2014). The parameters used to characterize non-uniform corrosion of reinforcement include maximum loss rate of cross-sectional area (Gao et al., 2019), maximum pit depth (Zhao et al., 2020), and the non-uniform coefficient of corrosion (ratio of average cross-sectional area to minimum cross-sectional area) (Zhang et al., 2014). Studies (Kashani et al., 2013; Stewart and Rosowsky, 1998; Zhang W. P. et al., 2021; Caleyo et al., 2009; Gu et al., 2018; Reshvanlou et al., 2022; Jin et al., 2020) have found that the residual cross-sectional areas of corroded rebars follows a normal distribution, lognormal distribution or Weibull distribution, and the ratio of minimum cross-sectional area to maximum cross-sectional area follows an extreme value type I (Gumble) distribution. The inhomogeneity coefficient R (average cross-sectional area to minimum cross-sectional area) approximately follows a Gumble distribution, generalized extreme value distribution or Frechet distribution. The pitting factor follows a lognormal distribution or an extreme value type I distribution. It is important to note that the aforementioned studies on the non-uniform corrosion characteristics of corroded rebars primarily rely on electrochemical accelerated corrosion tests and different researchers have reached varying conclusions regarding the distribution of non-uniform characterization parameters of corroded rebars.

Electrochemical accelerated corrosion tests can quickly produce corroded rebar samples, the non-uniform corrosion of which is different from that found in natural corroded components in the marine environment, leading to differences in the corrosion distribution characteristics of rebar surface (Otieno et al., 2013; Yuan et al., 2007; Ou et al., 2016). This paper investigates the apparent morphology characteristics of naturally corroded rebars in concrete under marine environmental conditions. Corroded rebars were extracted from actual engineering concrete structures,

and their precise morphology parameters were obtained using 3D scanning technology. The probability distribution models of residual cross-sectional areas and non-uniformity coefficient of naturally corroded rebars were studied to analyze the distribution and variation of these characteristic parameters under different corrosion levels.

2 Extraction of apparent morphology of corroded rebar

2.1 Samples of corroded rebar

Corroded rebar specimens were taken from the hollow beams of the approach bridge in a coastal pier, where the reinforced concrete members have been in service for 35 years, as shown in Figure 1. Field inspection indicates that nearly all the concrete cover of the bridge bottom surface show rust expansion, hollow bulging, spalling, exposed reinforcement and other deterioration, indicating serious rebar corrosion. The chloride ion content in the design depth of concrete cover has reached 0.15%, which far exceeds the critical threshold of rebar corrosion (ACI Committee 318, 1989). Nineteen HBR335 rebar samples with varying degrees of corrosion were extracted from the hollow beam, including nine rebars with a diameter of 20 mm and ten rebars with a diameter of 25 mm. Due to the difficulty of extracting longer specimens without causing damage and the time constraints during demolition, each rebar sample was cut into lengths of 450–500 mm.

2.2 Determination of corrosion rate and morphology

The corroded rebars were cleaned with dilute hydrochloric acid solution, neutralized with lime water solution, rinsed with clean water, and dried in a dryer for more than 4 h 3D scanning was performed on two uncorroded rebars and nineteen corroded rebars to obtain their 3D models (Figure 2). Additionally, cross-section of the 3D rebars models was taken at 1 mm intervals along the length of each rebar. In this paper, the average corrosion degree, or mass loss η_{ave}, of a corroded rebar is defined as Equation 1:

$$\eta_{ave} = \frac{A_0 - A_{av}}{A_0} \qquad (1)$$

where A_0 is the nominal cross-sectional area of an uncorroded rebar (mm^2), and A_{av} is the average cross-sectional area of a corroded rebar (mm^2). The maximum cross-sectional loss is located at the minimum residual cross-section with area of A_{min}, which is calculated by Equation 2:

$$\eta_{max} = \frac{A_0 - A_{min}}{A_0} \qquad (2)$$

The maximum pitting depth of corroded rebars was measured using a micrometer gauge, which has an accuracy of 0.01 mm. Two uncorroded rebars with diameters of 20 and 25 mm were selected as comparison samples, and numbered N20 and N25, respectively. Corroded rebars with different diameters are numbered 20-1 through 20-9 and 25-1 through 25-10 according to the average
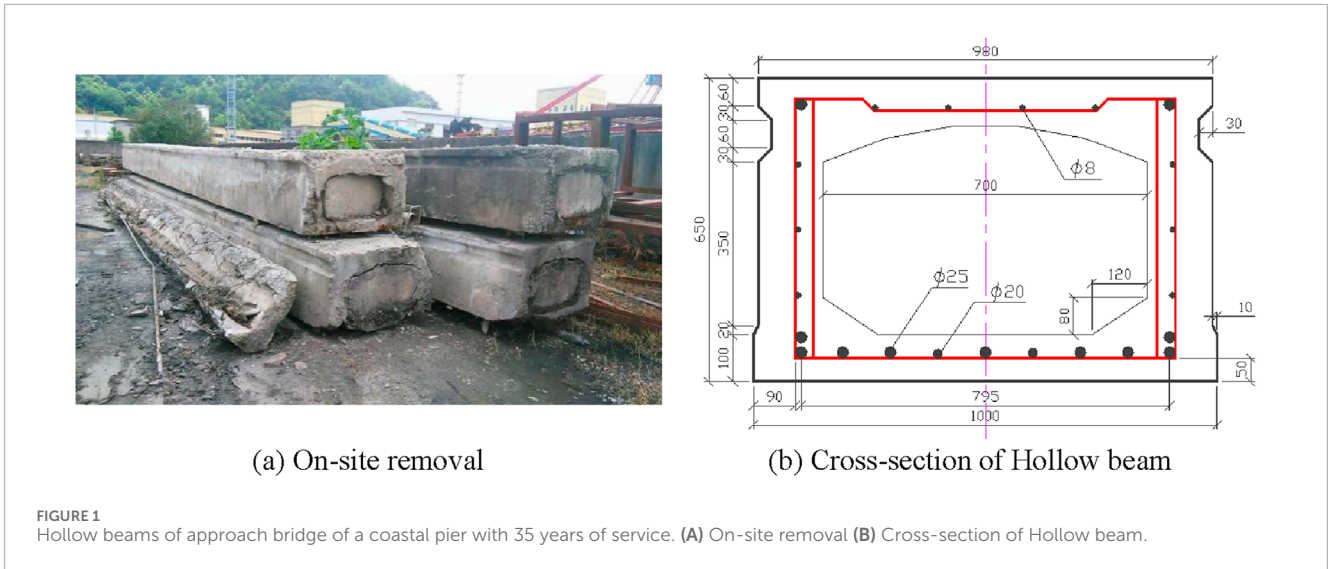
(a) On-site removal　　　　　　　　(b) Cross-section of Hollow beam

FIGURE 1
Hollow beams of approach bridge of a coastal pier with 35 years of service. **(A)** On-site removal **(B)** Cross-section of Hollow beam.
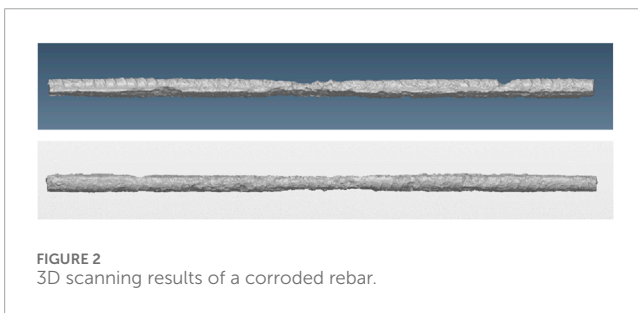

FIGURE 2
3D scanning results of a corroded rebar.

corrosion degree from smallest to largest. Table 1 lists the mass loss, maximum cross-sectional loss and maximum pitting depth of each corroded rebar. The mass loss η_{ave} of nineteen corroded rebars ranges from 7.58% to 24.96%, while the maximum cross-sectional loss η_{max} ranges from 24.72% to 55.62%.

3 Analysis of corrosion characteristics

3.1 Variation of the residual cross-sectional areas and pitting depth along the length

The residual cross-sectional areas of corroded rebars are a critical factor in determining their mechanical properties (Zeng et al., 2020). The non-uniform distribution of residual cross-sectional areas along the length of corroded rebars greatly increases the risk of structural failure. The current specification "Standard for durability assessment of existing concrete structures: GB/T 51355-2019" (GB/T 51355-2019, 2019), considers the cross-sectional loss rate and uniformity of corrosion as necessary conditions for determining the yield strength of corroded rebars.

The distribution of the residual cross-sectional areas along the length of the 20 mm rebars with varying corrosion levels is shown in Figure 3. Compared to the cross-sectional areas of the uncorroded rebar (N20), the residual cross-sectional areas of corroded rebars shows an obvious non-uniform distribution along

their length. When the mass loss is less than 10%, the residual cross-sectional areas of the rebars fluctuates around the average residual cross-sectional area, and the longitudinal and transverse ribs can be clearly identified on the rebars surface. When the mass loss exceeds 10%, the fluctuation amplitude of the residual cross-sectional areas increases with the corrosion rate, intensifying the non-uniform corrosion along the rebar's length. When the mass loss exceeds 15%, particularly when it surpasses 20%, the longitudinal and transverse ribs of the rebar nearly disappear on the rebars surface. The distribution of residual cross-sectional area in the 25 mm rebars is similar to that of the 20 mm rebars, and will not be repeated here.
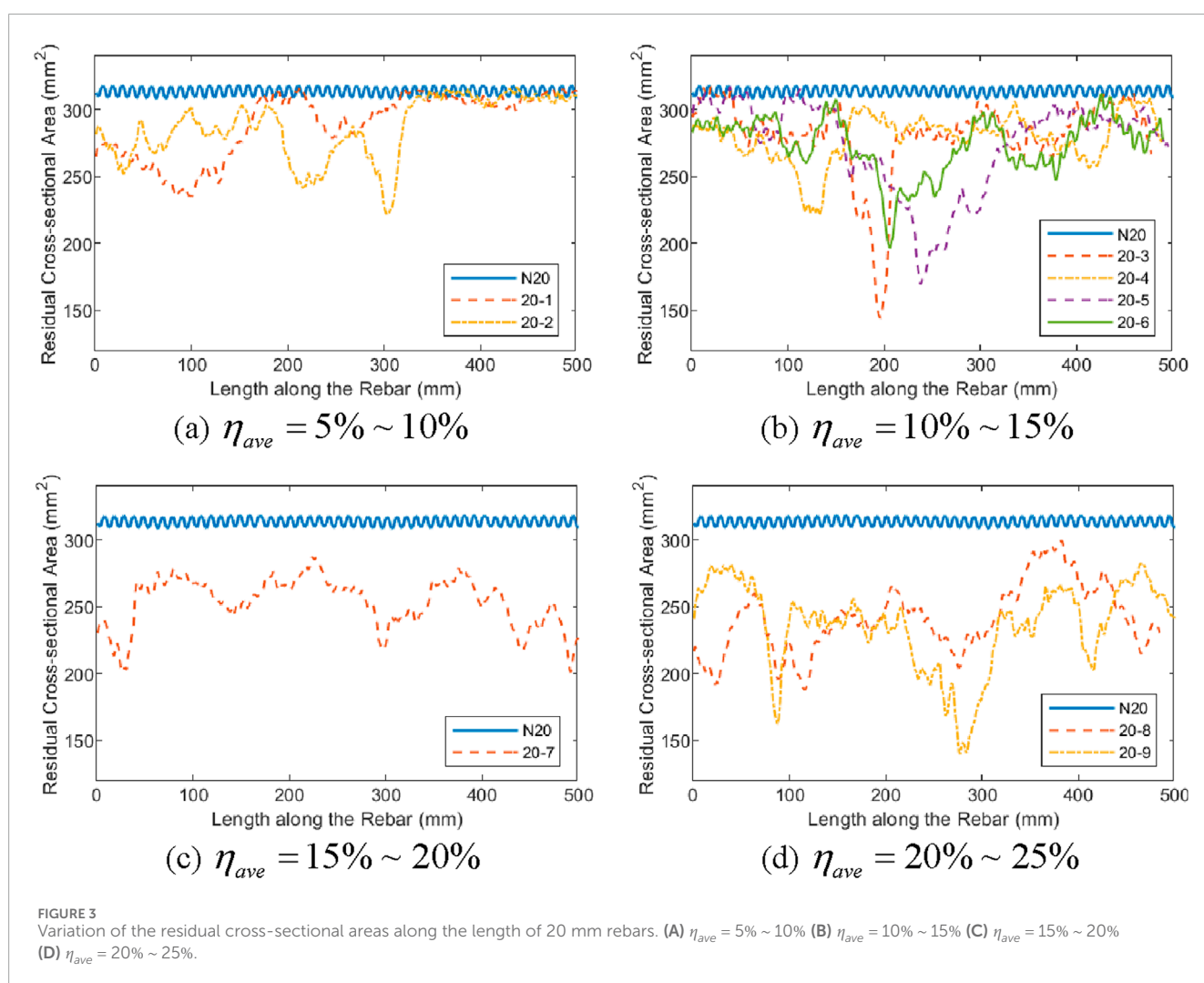
The decrease in the residual cross-sectional areas of rebars typically corresponds to the formation of new corrosion pits or an increase in pitting depth. Figure 4 presents the distribution of pitting depth along the length of four corroded rebars with different corrosion rates. It is evident that as the corrosion rate increases, the pitting depth becomes more irregular along the length of the rebar, with pits becoming larger and deeper.

3.2 Appearance of rebars after natural corrosion

To better understand the corrosion morphology characteristics of the rebar after natural corrosion, the longitudinal direction of the rebar is assumed to be the z-axis and the cross-section is represented in polar coordinates as the (r, θ), where r denotes the residual radius and θ represents the corresponding angle. A corroded rebar can then be unwrapped within the range $(-\pi \leq \theta \leq \pi)$ into a 3D surface plot and its overhead view, as shown in Figures 5A, B. The overhead view of 3D surface plot facilitates the observation of the overall changes in the corrosion morphology of the rebar along the longitudinal and circumferential directions. Additionally, Figure 5 illustrates the ribs pattern and the localized corrosion, which correspond to periodic peaks in the regions of low corrosion levels and significant valleys in the regions of high corrosion levels, respectively.
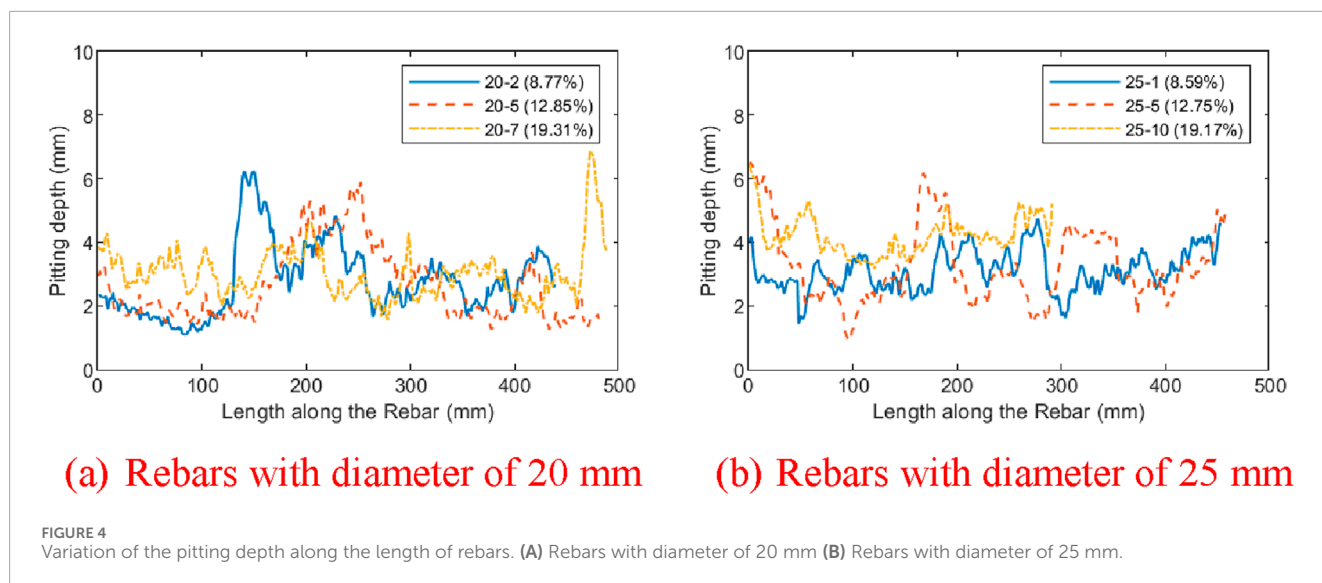
TABLE 1 Mass loss, maximum cross-section loss and maximum pitting depth of rebars.

	Unit	20-1	20-2	20-3	20-4	20-5	20-6	20-7	20-8	20-9	—
η_{ave}	%	7.58	8.77	10.55	11.13	12.80	12.85	19.31	23.23	24.96	—
η_{max}	%	25.38	29.45	54.12	29.57	46.17	37.62	36.05	40.28	55.62	—
Maximum pitting depth	mm	4.56	6.24	8.67	4.61	5.9	4.66	6.87	6.53	8.17	
	Unit	25-1	25-2	25-3	25-4	25-5	25-6	25-7	25-8	25-9	25-10
η_{ave}	%	8.59	9.91	11.08	12.11	12.75	12.89	13.13	17.30	17.70	19.17
η_{max}	%	21.92	31.57	31.79	37.59	39.02	50.14	24.72	31.69	43.84	37.77
Maximum pitting depth	mm	4.75	7.15	5.68	8.32	6.51	11.05	4.94	6.25	9.81	6.46

(a) $\eta_{ave} = 5\% \sim 10\%$

(b) $\eta_{ave} = 10\% \sim 15\%$

(c) $\eta_{ave} = 15\% \sim 20\%$

(d) $\eta_{ave} = 20\% \sim 25\%$

FIGURE 3
Variation of the residual cross-sectional areas along the length of 20 mm rebars. **(A)** η_{ave} = 5% ~ 10% **(B)** η_{ave} = 10% ~ 15% **(C)** η_{ave} = 15% ~ 20%
(D) η_{ave} = 20% ~ 25%.

Figures 6, 7 depict the non-uniform corrosion of corroded rebar 20-6 with 12.85% mass loss and the pitting corrosion of corroded rebar 25-2 with 9.91% mass loss. The red square and black circular wireframes highlight the corresponding corrosion characteristics as seen from the perspective of 3D scanning

model and the maximum pit depth cross-section, respectively. The variations of cross-sections along the rebars, as shown in Figures 6A, 7A, illustrate that the residual cross-sectional shapes of corroded rebars are directly related to their position within concrete members. The corrosion zones of rebars predominantly occur on

(a) Rebars with diameter of 20 mm　　**(b) Rebars with diameter of 25 mm**

FIGURE 4
Variation of the pitting depth along the length of rebars. **(A)** Rebars with diameter of 20 mm **(B)** Rebars with diameter of 25 mm.

the side adjacent to the concrete cover, displaying noticeable uneven corrosion characteristics in the residual cross-sectional shape of the rebars.

4 Characteristics of residual cross-sectional areas

4.1 Probability distribution of residual cross-sectional areas of a single rebar

The probability distribution model of the residual cross-sectional areas is crucial for predicting the load-carrying capacity of corroded reinforced concrete (Maslehuddin et al., 1990). To facilitate comparative analysis, the residual cross-sectional areas of each rebar are normalized to their corresponding nominal areas. The residual cross-sectional areas of 19 corroded rebar specimens were statistically analyzed to further quantify their distribution characteristics, and several common probability distribution models were selected to fit the test data. These models include normal distribution, lognormal distribution, generalized extreme value (GEV) distribution. Based on the value of shape parameter, GEV distribution can be categorized into type I, type II and type III extreme value distribution (Millington et al., 2011). When the shape parameter is non-zero, the probability density function (PDF) and Cumulative distribution function (CDF) for the GEV distribution are, respectively, expressed as Equations 3 and 4:

$$f(A) = \left(\frac{1}{\sigma}\right) \exp\left(-\left(1 + k\frac{(A-\mu)}{\sigma}\right)^{-1/k}\right)\left(1 + k\frac{(A-\mu)}{\sigma}\right)^{-1-1/k} \quad (3)$$

$$F(A) = \exp\left(-\left(1 + k\left(\frac{A-\mu}{\sigma}\right)^{-1/k}\right)\right) \quad (4)$$

Where A is the normalized cross-sectional areas along the length of a rebar, k, μ and σ are shape parameter, position parameter and scale parameter, respectively. When $k < 0$, the

GEV distribution is the type III extreme value, or three-parameter Weibull, distribution. In the case of $k > 0$, the GEV distribution is the type II extreme value, or three-parameter Frechet, distribution. In the limit as k approaches 0, the GEV is the mirror image of the type I extreme value, or Gumbel, distribution, the probability density function of which is given by Equation 5:

$$f(A) = \frac{1}{\sigma} \cdot \exp\left(-\exp\left(-\frac{A-\mu}{\sigma}\right) - \frac{A-\mu}{\sigma}\right) \quad (5)$$

Figure 8 displays the statistical histogram plot of the normalized areas and optimal distribution of the residual cross-sections for typical specimens. The histograms of the residual cross-sectional areas under varying corrosion degrees predominantly exhibit an asymmetric negative skew distribution, as illustrated in Figures 8A, B. Notably, the histogram of rebar 20-3 (Figure 8C) shows a pronounced left-skewed tail that is heavier than that of a normal distribution. This phenomenon suggests the presence of localized, unusually severe pitting in the rebar. The histogram characteristics of rebar 25-6 are similar to those of rebar 20-3 (Figure 8D). Under the condition of low mass loss (10%~13%), the maximum cross-sectional loss of rebars 20-3 and 25-6 exceeds 50%, rendering these cross-sections the weakest points in the rebars. The distribution of the cross-sections along the length of a corroded rebar is highly uneven, and the average corrosion loss of rebars taken from different positions within the same concrete structure varies significantly. A similar conclusion was reached by Zhang J. Z. et al. (2021). Therefore, assessing the durability of a concrete structure solely by examining a section of rebar may not be reliable.

The Kolmogorov-Smirnov (K-S) test (Fasano and Franceschini, 1987) was conducted at a 95% confidence level to preliminarily estimate the appropriate distribution model for the cross-sectional areas of corroded rebars. Table 2 presents the results of K-S test and maximum likelihood estimates of the parameters for the GEV distribution, revealing that 68% of the corroded rebar samples conform to the GEV distribution, 16% conform to both the lognormal and normal distribution, and 32% do
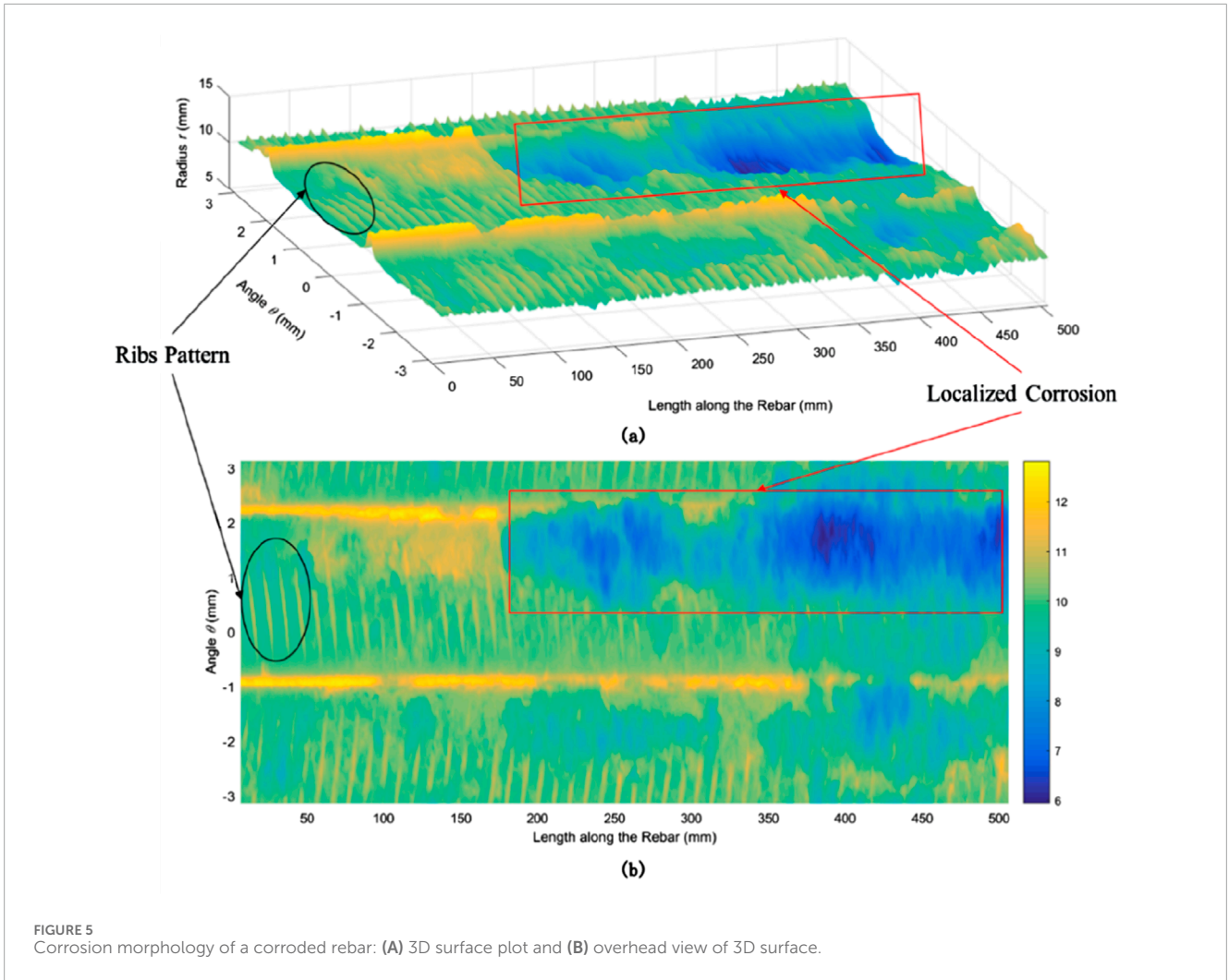
FIGURE 5
Corrosion morphology of a corroded rebar: **(A)** 3D surface plot and **(B)** overhead view of 3D surface.
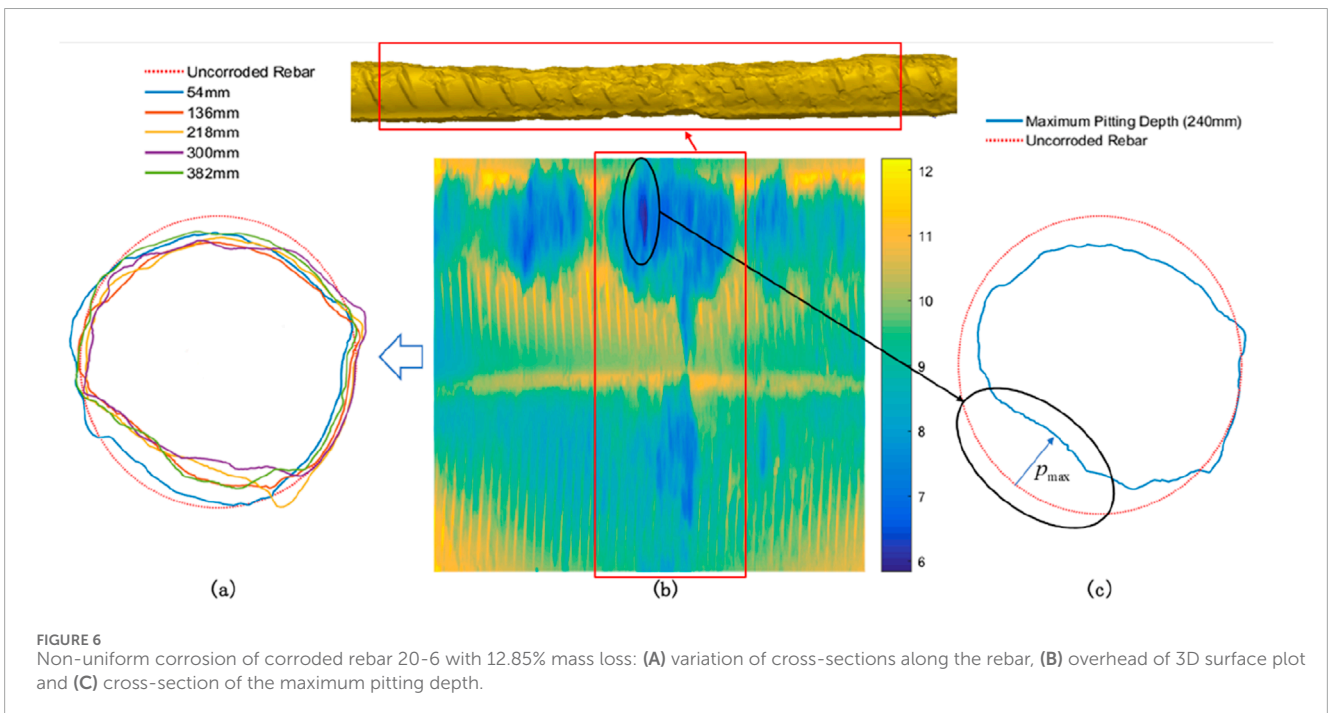

FIGURE 6
Non-uniform corrosion of corroded rebar 20-6 with 12.85% mass loss: **(A)** variation of cross-sections along the rebar, **(B)** overhead of 3D surface plot and **(C)** cross-section of the maximum pitting depth.
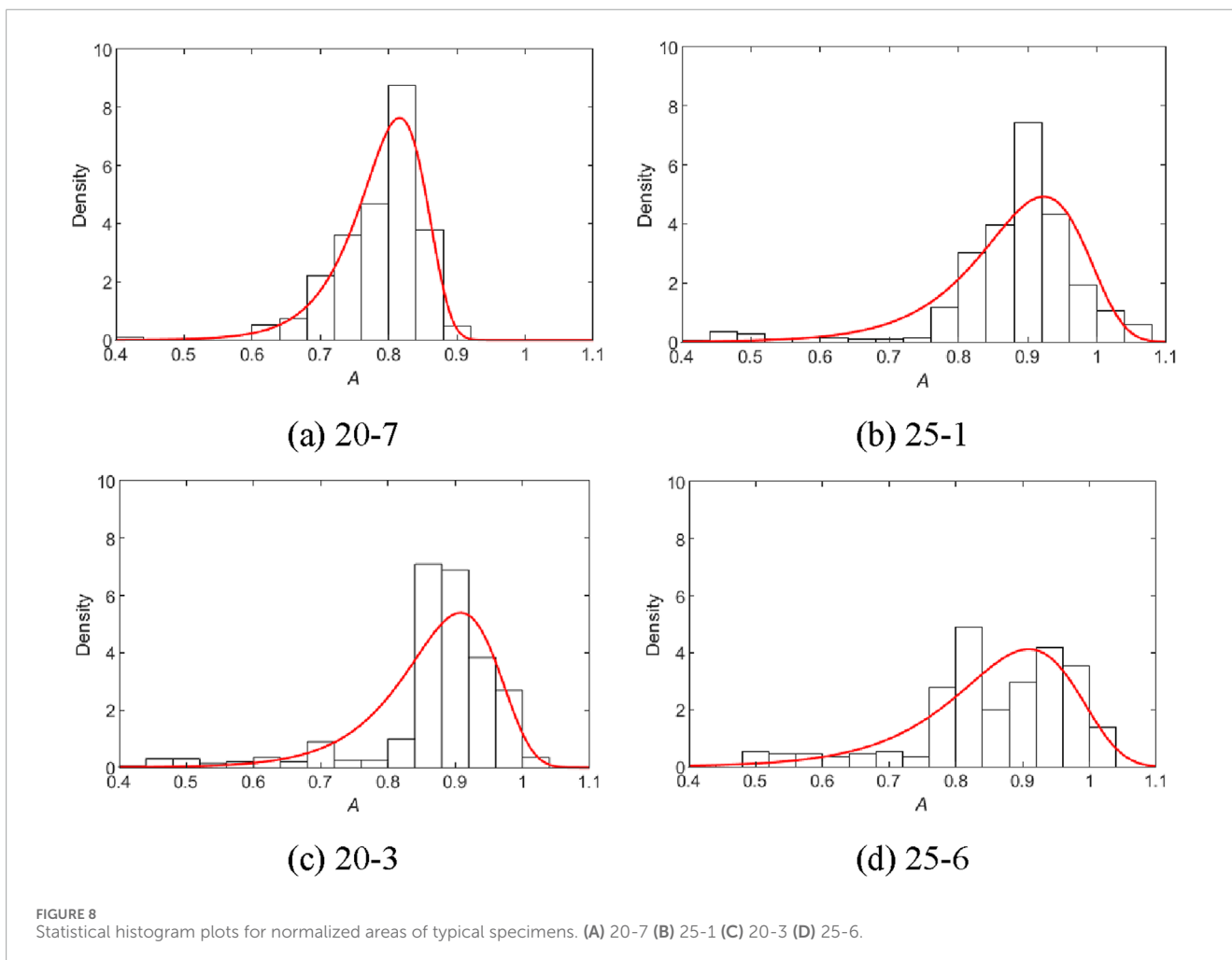
FIGURE 7
Pitting corrosion of corroded bar 25-2 with 9.91% mass loss: **(A)** variation of cross-section cuts along the bar, **(B)** overhead view of 3D surface plot and **(C)** cross-section of the maximum pitting depth.

FIGURE 8
Statistical histogram plots for normalized areas of typical specimens. **(A)** 20-7 **(B)** 25-1 **(C)** 20-3 **(D)** 25-6.
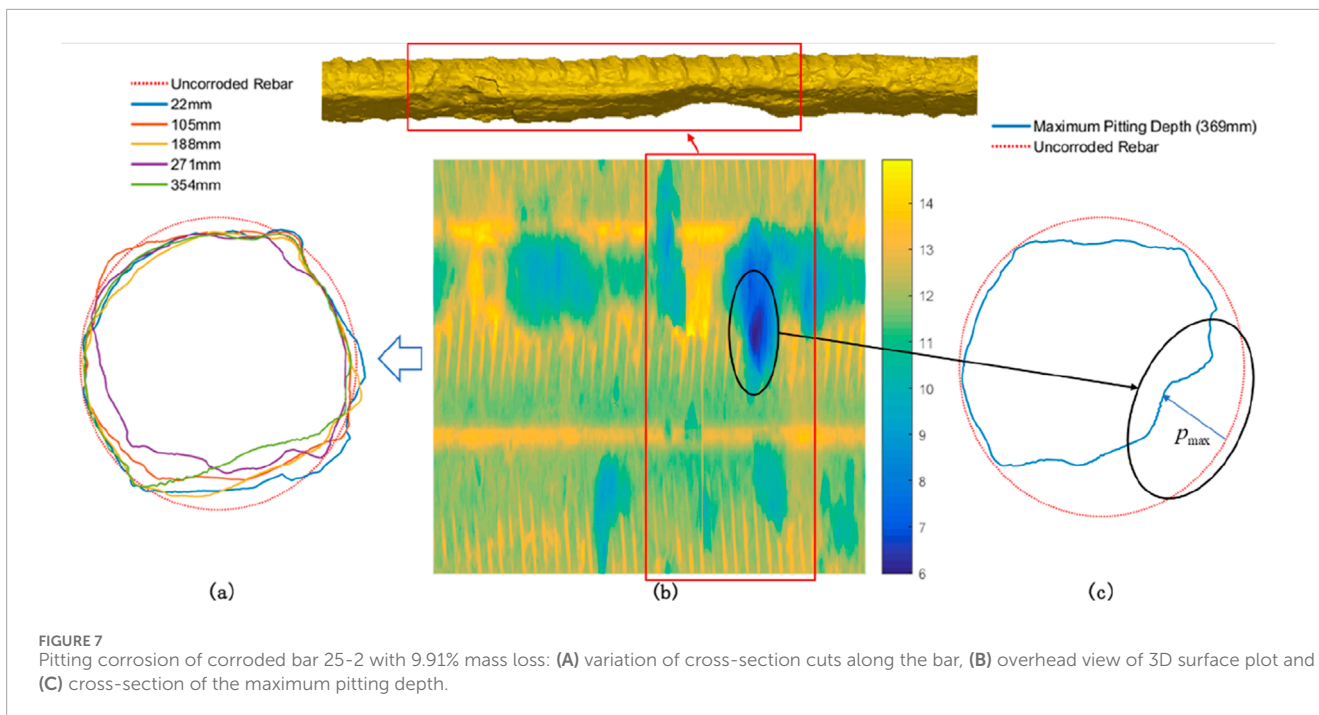
TABLE 2 Results of K-S test and maximum likelihood estimates of the parameters for the GEV distribution.

| Samples	K-S test			Parameters		
	Normal	Lognormal	GVE	k	μ	σ
20-1	Yes	Yes	No	−0.6745	0.0981	0.8527
20-2	Yes	Yes	Yes	−0.9179	0.0825	0.9204
20-3	Yes	Yes	No	−0.7931	0.0817	0.9053
20-4	Yes	Yes	No	−0.6481	0.1085	0.7342
20-5	Yes	Yes	No	−0.5119	0.0636	0.7931
20-6	Yes	Yes	No	−0.5764	0.0620	0.8776
20-7	Yes	Yes	No	−0.5215	0.0727	0.8560
20-8	Yes	Yes	Yes	−0.7248	0.0924	0.8829
20-9	No	No	No	−0.2319	0.0783	0.7375
25-1	Yes	Yes	Yes	−0.7688	0.1153	0.8603
25-2	Yes	Yes	No	−0.6931	0.0950	0.8610
25-3	No	No	No	−0.5415	0.0493	0.8602
25-4	Yes	Yes	No	−0.6211	0.0761	0.8778
25-5	Yes	Yes	Yes	−0.6428	0.0767	0.7981
25-6	Yes	Yes	No	−0.6768	0.0711	0.8925
25-7	Yes	Yes	No	−0.7244	0.0836	0.8700
25-8	Yes	Yes	Yes	−1.0280	0.1287	0.8719
25-9	No	No	No	−0.5868	0.0562	0.9051
25-10	Yes	Yes	Yes	−0.4164	0.0991	0.8010

not conform to any distribution examined in this study. For corroded rebars with a truncated length of 500 mm, the residual cross-sectional areas do not follow any specific distribution, and there is no apparent correlation between the corrosion rate and its distribution pattern. Based on the proportions of samples fitting each probability distribution model, GVE distribution with $k < 0$, or three-parameter Weibull distribution best represents the distribution for residual cross-sectional areas of corroded rebars.

4.2 Influence of different diameters on corrosion of rebars

The average mass losses for 20 and 25 mm corroded rebar samples are 14.66% and 13.51%, respectively, while the maximum cross-sectional losses are 55.62% and 50.14%. Figure 9 presents the graphic analysis of the residual cross-sectional areas of the rebars with diameter of 20 and 25 mm, including histogram,

quantile-quantile (Q-Q) and cumulative distribution function plots. Various probability distribution models are compared for the residual cross-sectional areas of 20 and 25 mm corroded rebar samples, as illustrated by the histogram plots in Figure 9. It can be concluded that GVE distribution with $k < 0$, or three-parameter Weibull distribution best fits the residual cross-sectional areas of corroded rebar samples with different diameters. The Q-Q and CDF plots demonstrate the goodness-of-fit of GVE distribution with $k < 0$, or three-parameter Weibull distribution. Additionally, the GVE distributions for both rebar diameters are supported by the K-S test at a 95% confidence level.

After normalizing the residual cross-sectional areas of corroded rebar samples with different diameters, all the data still conform to the GVE distribution model with shape parameter $k = -0.6201$, position parameter $\mu = 0.8429$ and scale parameter $\sigma = 0.1039$. The probability density and distribution functions are illustrated in Figure 10. Both rebar samples, despite their diameters, are tensile rebars located at the bottom of the members and exposed to the same
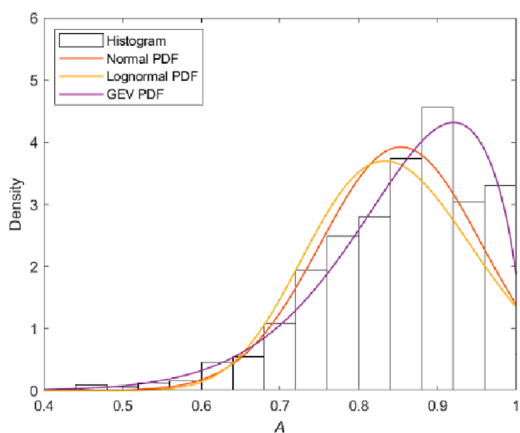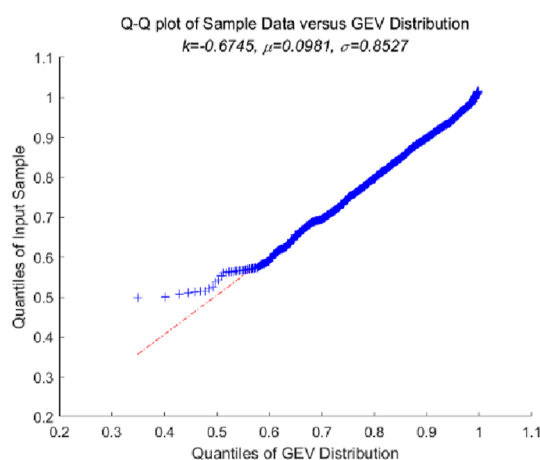
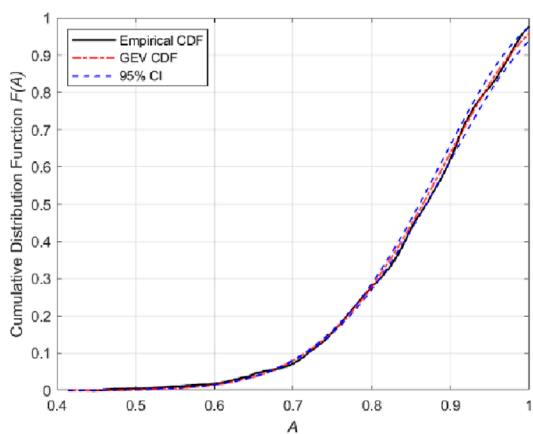(a) Histogram plot of the 20 mm corroded rebar samples
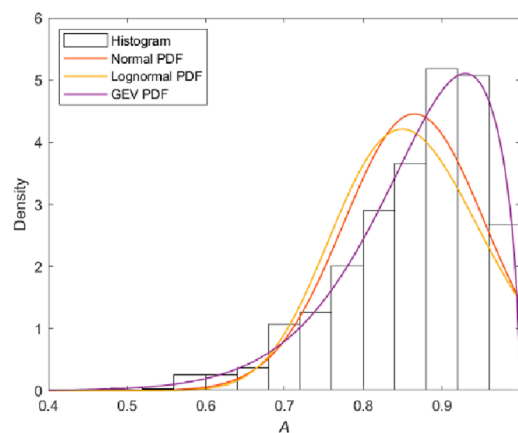
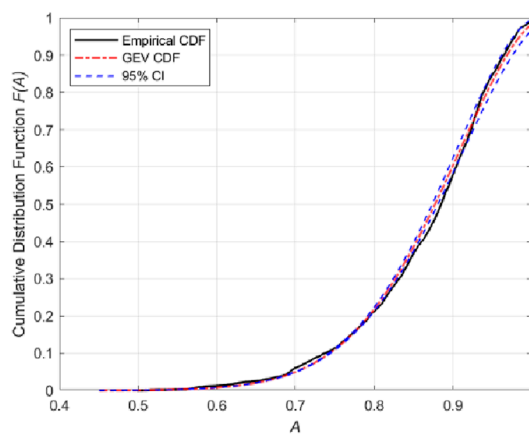(b) Histogram plot of the 25 mm corroded rebar samples
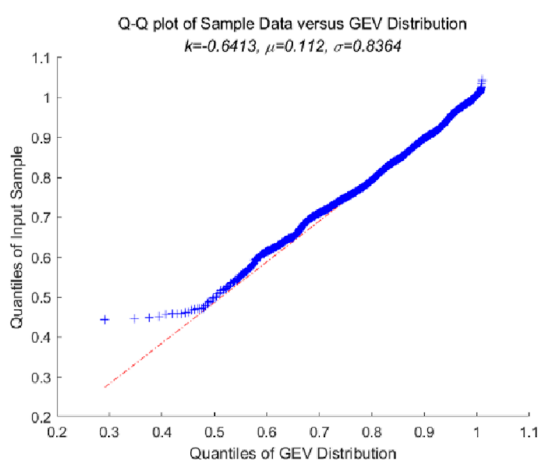
(c) Q-Q plot of the 20 mm corroded rebar samples

(d) Q-Q plot of the 25 mm corroded rebar samples

(e) CDF plot of the 20 mm corroded rebar samples

(f) CDF plot of the 25 mm corroded rebar samples

FIGURE 9
Graphic analysis of the probability distributions for the residual cross-sectional areas of corroded rebars with diameter of 20 and 25 mm. **(A)** Histogram plot of the 20 mm corroded rebar samples **(B)** Histogram plot of the 25 mm corroded rebar samples **(C)** Q-Q plot of the 20 mm corroded rebar samples **(D)** Q-Q plot of the 25 mm corroded rebar samples **(E)** CDF plot of the 20 mm corroded rebar samples **(F)** CDF plot of the 25 mm corroded rebar samples.

FIGURE 10
Graphic analysis of the probability distributions for the residual cross-sectional areas of all corroded rebar samples. **(A)** Histogram plot of all corroded rebar samples **(B)** Q-Q plot of all corroded rebar samples **(C)** CDF plot of all corroded rebar samples.
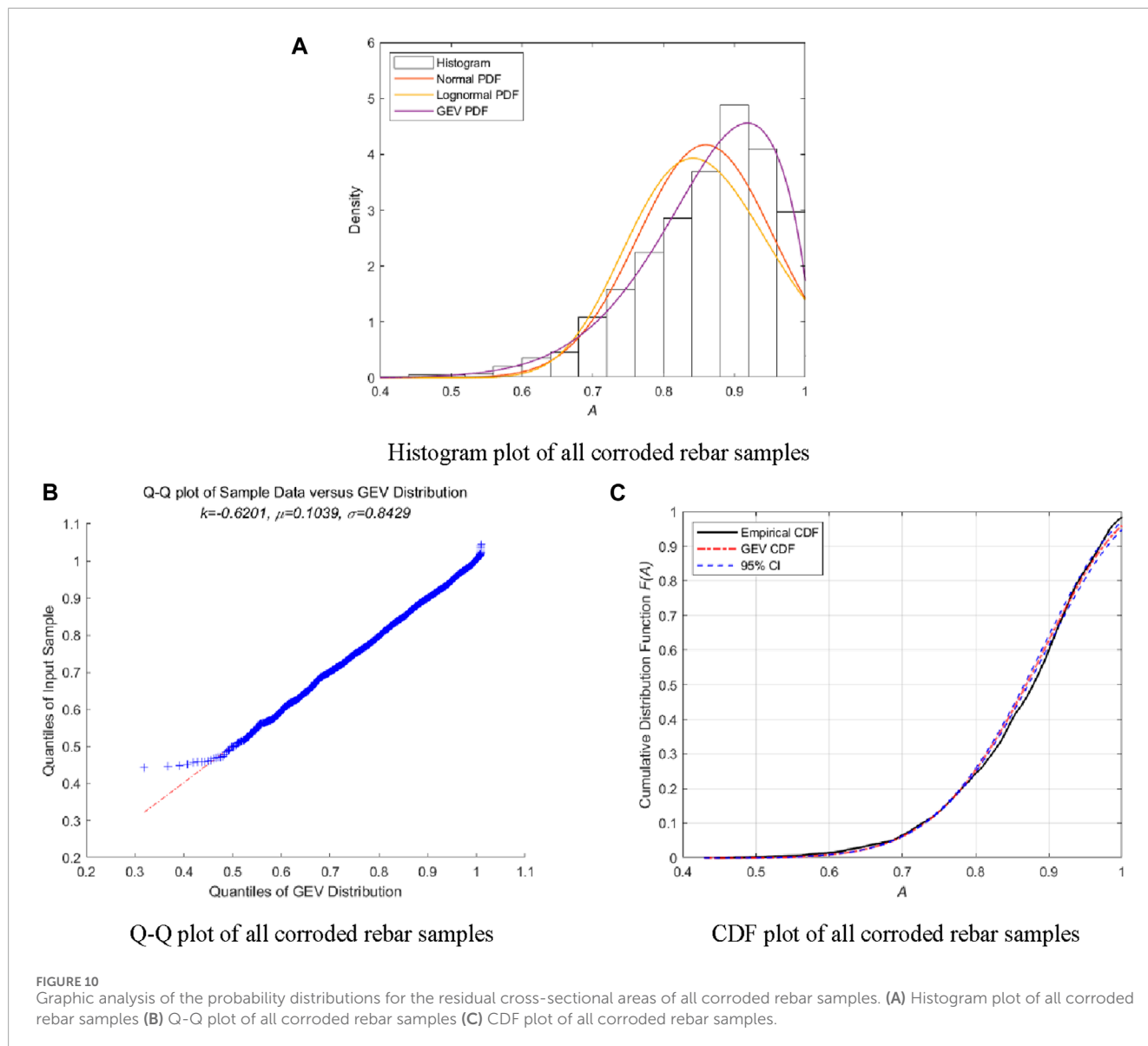
corrosion environment. As shown in Figures 9, 10, the diameter of corroded rebars has minimal influence on the degree and form of corrosion experienced by rebars in the same member in the marine environment.

Indeed, the effect of rebar diameter on corrosion remains inconclusive. On one hand, using larger diameter rebars with the same reinforcement ratio can decrease the specific surface area of the bars exposed to corrosion, thereby reducing both the degree and non-uniformity of corrosion under the same environmental and temporal conditions (Gu et al., 2018). On the other hand, a larger reinforcement diameter increases the risk of cracking in the concrete cover, which causes premature cracking and accelerates the corrosion process of the reinforcement (Chen et al., 2019). However, these conclusions are primarily based on samples of corroded steel bars obtained from accelerated laboratory tests, rather than the naturally corroded prototype members analyzed in this paper.

5 Spatial heterogeneity factor

5.1 Definition of spatial heterogeneity factor

Currently, the ratio of average cross-sectional area to the minimum cross-sectional area of a corroded rebar is commonly used to define the spatial heterogeneity factor R of the corroded rebar. This factor reflects the relationship between the maximum cross-sectional loss and the mass loss of a corroded rebar sample, highlighting the non-uniform corrosion along the longitudinal axis of corroded rebars. Previous research has shown that (Gu et al., 2018), when the unit length of the corroded rebar is between 30 and 50 mm, the autocorrelation coefficient of the spatial heterogeneity factor is generally less than 0.3, indicating a weak correlation. Therefore, in this paper, a 50 mm analysis length is selected, and Equation 6 is used to calculate the spatial
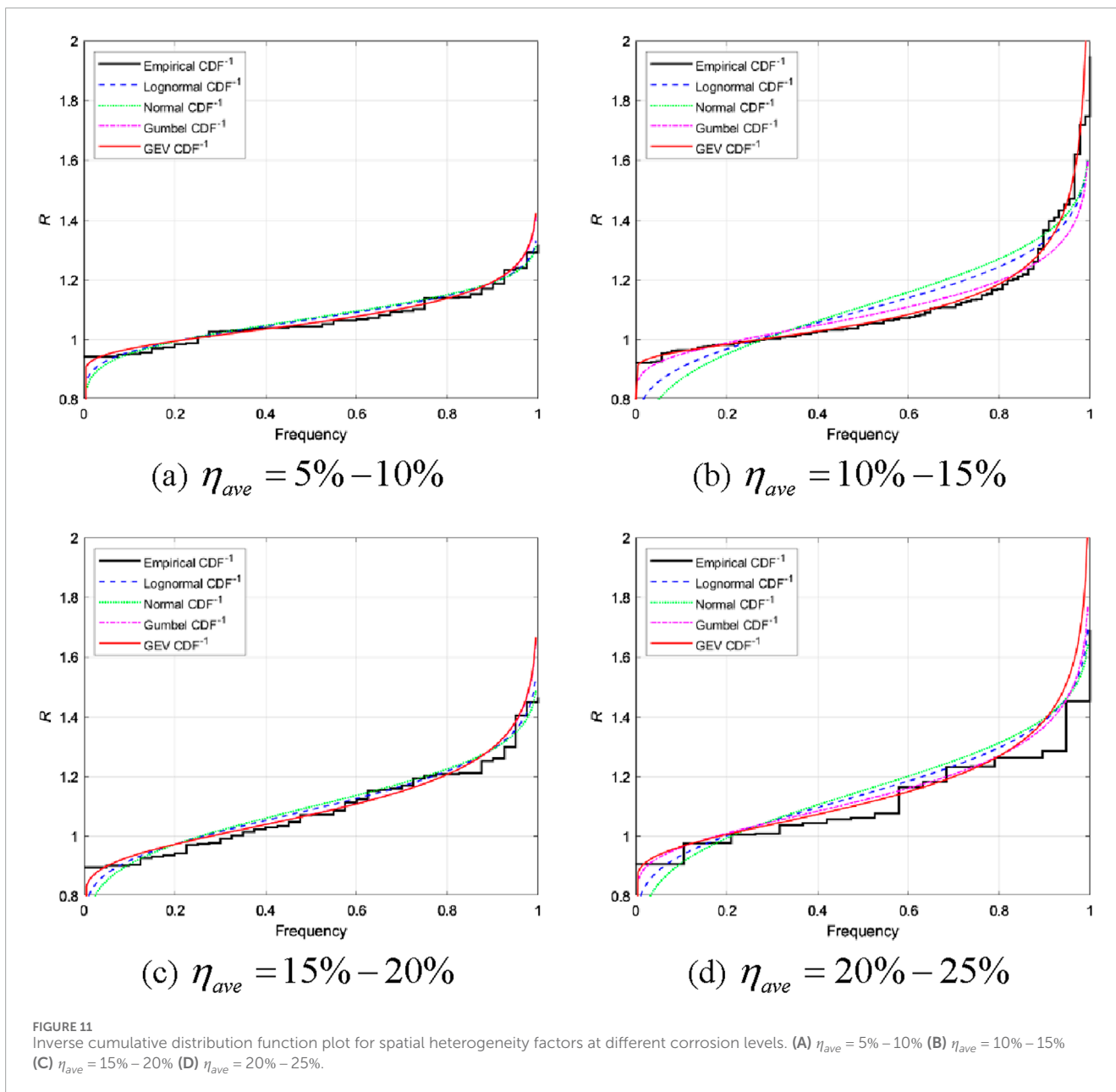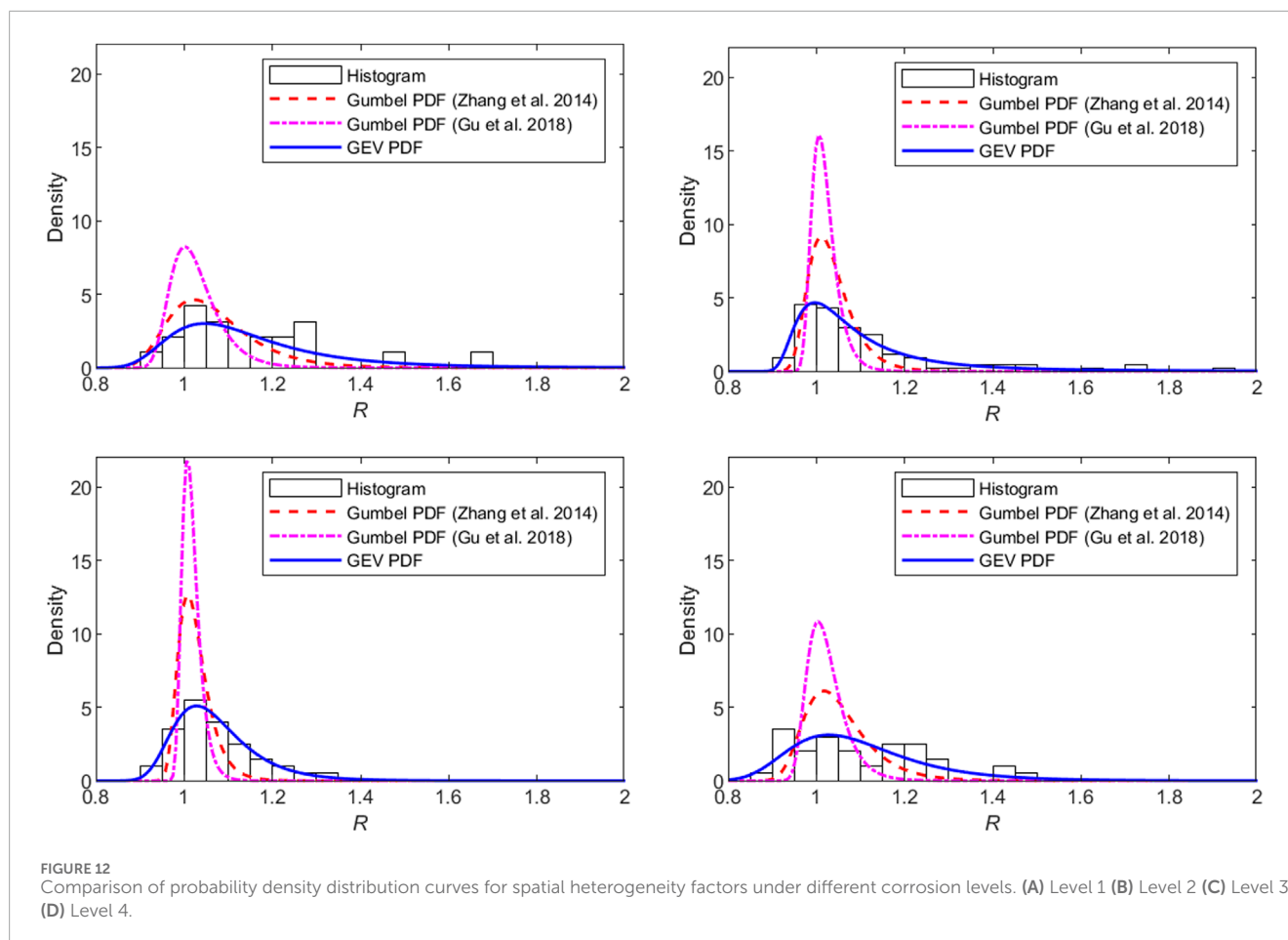
FIGURE 11
Inverse cumulative distribution function plot for spatial heterogeneity factors at different corrosion levels. **(A)** $\eta_{ave} = 5\% - 10\%$ **(B)** $\eta_{ave} = 10\% - 15\%$ **(C)** $\eta_{ave} = 15\% - 20\%$ **(D)** $\eta_{ave} = 20\% - 25\%$.

TABLE 3 Parameters estimation of GEV distribution under different corrosion levels.

Level	Corrosion degrees of rebar samples (%)	η_{ave} (%)	η_{max} (%)	Parameters		
				k	μ	σ
1	5–10	8.83	31.57	0.0122	1.0288	0.0722
2	10–15	12.19	50.14	0.3587	1.0207	0.0835
3	15–20	18.28	43.84	0.0079	1.029	0.118
4	20–25	24.14	55.62	0.1444	1.0629	0.1233

FIGURE 12
Comparison of probability density distribution curves for spatial heterogeneity factors under different corrosion levels. **(A)** Level 1 **(B)** Level 2 **(C)** Level 3 **(D)** Level 4.

heterogeneity factor (Zhang et al., 2014).

$$R = \frac{A_{ave}}{A_{\min,50}} \qquad (6)$$

where $A_{\min,50}$ is the minimum residual cross-sectional area within each element of analysis length (mm^2).

5.2 Probability distribution of spatial heterogeneity factors

The probability distribution of spatial heterogeneity factors can be applied to time-varying reliability analysis of corroded reinforced concrete beams. The Gumbel distribution has been reported to be the best fit to the spatial heterogeneity factors of accelerated corroded rebars (Zhang et al., 2014; Zhang W. P. et al., 2021; Gu et al., 2018). However, the mechanism of the accelerated corrosion differs from natural corrosion in that it imposes a higher corrosion rate, which does not correspond to the equilibrium mixed potential found under typical service conditions (Gonzalez et al., 1995). There remains a lack of in-depth research on the probability distribution of spatial heterogeneity factors in naturally corroded rebars.

Given that the actual statistical length of each rebar sample is approximately 450–500 mm, these corroded rebar samples can

be divided into equal-length units of 50 mm to meet the data volume requirements for parameter fitting and account for the actual length of the rebars. Based on different corrosion levels, the inverse cumulative distribution function (CDF^{-1}) plot, commonly known as the quantile plot (Rosenkrantz, 2000; Xiao, 2015), is employed to fit probability distributions, such as normal distribution, lognormal distribution, and GEV distribution, to the data of the spatial heterogeneity factors R, as illustrated in Figure 11. It can be observed that the GVE distribution model with $k > 0$, or the three-parameter Frechet distribution, exhibits good adaptability to the spatial heterogeneity factor R across different corrosion levels. In addition, the three-parameter Frechet distributions for the spatial heterogeneity factors R at different corrosion levels is supported by K-S test at a significance level of 95% confidence.

5.3 Relationship between spatial heterogeneity factors and corrosion levels

The deterioration of mechanical properties in corroded rebars, influenced by longitudinal non-uniformity, should be treated as a time-dependent factor to accurately reflect the impact of different corrosion levels (Zhang W. P. et al., 2021). As corrosion progresses over time, the non-uniform loss of material along the length of the rebar significantly alters its load-bearing capacity and structural

integrity, emphasizing the need for establishing the relationship between spatial heterogeneity factors and corrosion levels.

Table 3 lists the estimated parameters of GEV distribution for spatial heterogeneity factor R under different corrosion levels. As seen in Table 3, the position parameter μ increases with rising corrosion levels, indicating that higher average corrosion levels of a corroded rebar may result in larger spatial heterogeneity factors on the rebar surface. On the other hand, the scale parameter σ shows a generally increasing trend with higher corrosion levels, suggesting that the greater corrosion correspond to increased dispersion in the spatial heterogeneity factors. Higher corrosion levels tend to shift the distribution curve towards higher heterogeneity factors, illustrating that the non-uniformity and spatial variability increase with corrosion.

To facilitate comparison with previous studies, the corresponding probability distribution function curves are presented in Figure 12. In these figures, the statistical histograms and blue solid lines represent the sample data and the corresponding GEV distributions of naturally corroded deformed rebars from this study. The red dotted lines represent the fitting results of Zhang et al. (2014) for accelerated corroded plain round rebars with a diameter of 20 mm, while the purple dotted lines represent the fitting results of Gu et al. (2018) for accelerated corroded deformed rebars with a diameter of 16 mm. Figure 12 illustrates that the spatial heterogeneity factors for different types of rebars in various environments exhibit distinct distribution patterns. For deformed rebars naturally corroded in the marine environment, the three-parameter Frechet distribution, more effectively characterizes probability density distributions for spatial heterogeneity factors under different corrosion levels.

6 Conclusion

(1) In the marine environment, corrosion of a rebar primarily occurs on the side adjacent to the concrete surface, predominantly in the form of non-uniform or pitting corrosion along the length and cross-section direction of rebars. Thus, evaluating structural durability based on a single section of rebar is unreliable.

(2) The residual cross-sectional areas of naturally corroded rebars in concrete structures generally follow a type III extreme value distribution, or a three-parameter Weibull distribution. However, no specific probability distribution model or clear correlation with the distribution pattern exists for rebars with varying corrosion levels.

(3) A comparison of the corrosion characteristics of rebars with different diameters in the same concrete member reveals that,

in the same service environment, rebar diameter has minimal influence on the corrosion degree and form of corrosion in marine concrete members.

(4) In the marine environment, the spatial heterogeneity factors of naturally corroded rebars follow a type II extreme value distribution, or a three-parameter Frechet distribution. As corrosion progresses, both the position and scale parameters of the distribution function exhibit an increasing trend.

Data availability statement

The data that support the findings of this study are available from the corresponding authors upon reasonable request.

Author contributions

Funding

Conflict of interest

Authors ZY, JL, and JZ were employed by CCCC Fourth Harbor Engineering Institute Co., Ltd.

Publisher's note

All claims expressed in this article are solely those of the authors and do not necessarily represent those of their affiliated organizations, or those of the publisher, the editors and the reviewers. Any product that may be evaluated in this article, or claim that may be made by its manufacturer, is not guaranteed or endorsed by the publisher.

References

ACI Committee 318 (1989). *Building code requirements for reinforced concrete and commentary (ACI 318-89/ACI 318R-89)*. Detroit: American Concrete Institute.

Almusallam, A. A. (2001). Effect of degree of corrosion on the properties of reinforcing steel bars. *Constr. Build. Mater* 15, 361–368. doi:10.1016/s0950-0618(01)00009-5

Apostolopoulos, C. A., Demis, S., and Papadakis, V. G. (2013). Chloride-induced corrosion of steel reinforcement – mechanical performance and pit depth analysis. *Constr. Build. Mater* 38AD, 139–146. doi:10.1016/j.conbuildmat.2012.07.087

Bazant, Z. P. (1979). Physical model for steel corrosion in concrete sea structures - application. *J. Struct. Div.* 105, 1155–1166. doi:10.1061/jsdeag.0005169

Bhargava, K., Ghosh, A. K., Mori, Y., and Ramanujam, S. (2007). Corrosion-induced bond strength degradation in reinforced concrete - analytical and empirical models. *Nucl. Eng. Des.* 237, 1140–1157. doi:10.1016/j.nucengdes.2007.01.010

Caleyo, F., Velázquez, J. C., Valor, A., and Hallen, J. M. (2009). Probability distribution of pitting corrosion depth and rate in underground pipelines: a Monte Carlo study. *Corros. Sci.* 51, 1925–1934. doi:10.1016/j.corsci.2009.05.019

Chen, J., Zhang, W., and Gu, X. (2019). Modeling time-dependent circumferential non-uniform corrosion of steel bars in concrete considering corrosion-induced cracking effects. *Eng. Struct.* 201, 109766. doi:10.1016/j.engstruct.2019.109766

Costa, A., and Appleton, J. (2002). Case studies of concrete deterioration in a marine environment in Portugal. *Cem. Concr. Compos* 24, 169–179. doi:10.1016/s0958-9465(01)00037-3

Du, Y. G., Clark, L. A., and Chan, A. H. C. (2005). Residual capacity of corroded reinforcing bars. *Mag. Concr. Res.* 57, 135–147. doi:10.1680/macr.2005.57.3.135

Fasano, G., and Franceschini, A. (1987). A multidimensional version of the Kolmogorov–Smirnov test. *Mon. Not. R. Astron Soc.* 225, 155–170. doi:10.1093/mnras/225.1.155

Fernandez, I., Lundgren, K., and Zandi, K. (2018). Evaluation of corrosion level of naturally corroded bars using different cleaning methods, computed tomography, and 3D optical scanning. *Mater Struct.* 51, 78. doi:10.1617/s11527-018-1206-z

Francois, R., Khan, I., and Dang, V. H. (2013). Impact of corrosion on mechanical properties of steel embedded in 27-year-old corroded reinforced concrete beams. *Mater Struct.* 46, 899–910. doi:10.1617/s11527-012-9941-z

Gao, X., Pan, Y., and Ren, X. (2019). Probabilistic model of the minimum effective cross-section area of non-uniform corroded steel bars. *Constr. Build. Mater* 216, 227–238. doi:10.1016/j.conbuildmat.2019.05.012

GB/T 51355-2019 (2019). *Standard for durability assessment of existing concrete structures: GB/T 51355-2019*. Beijing: China Architecture and Building Press.

Gonzalez, J. A., Andrade, C., Alonso, C., and Feliu, S. (1995). Comparison of rates of general corrosion and maximum pitting penetration on concrete embedded steel reinforcement. *Cem. Concr. Res.* 25 (2), 257–264. doi:10.1016/0008-8846(95)00006-2

Gu, X., Guo, H., Zhou, B., Zhang, W., and Jiang, C. (2018). Corrosion non-uniformity of steel bars and reliability of corroded RC beams. *Eng. Struct.* 167, 188–202. doi:10.1016/j.engstruct.2018.04.020

Jin, N. G., He, J. H., Fu, C. Q., and Jin, X. Y. (2020). Study on experimental method and morphology of accelerated non-uniform corrosion of steel bars. *J. Zhejiang Univ. Eng. Sci.* 54, 8. doi:10.3785/j.issn.1008-973X.2020.03.008

Kashani, M. M., Crewe, A. J., and Alexander, N. A. (2013). Use of a 3D optical measurement technique for stochastic corrosion pattern analysis of reinforcing bars subjected to accelerated corrosion. *Corros. Sci.* 73, 208–221. doi:10.1016/j.corsci.2013.03.037

Lim, S., Akiyama, M., Frangopol, D. M., and Jiang, H. (2017). Experimental investigation of the spatial variability of the steel weight loss and corrosion cracking of reinforced concrete members: novel X-ray and digital image processing techniques. *Struct. Infrastruct. Eng.* 13, 118–134. doi:10.1080/15732479.2016.1198397

Malumbela, G., Alexander, M., and Moyo, P. (2010). Variation of steel loss and its effect on the ultimate flexural capacity of RC beams corroded and repaired under load. *Constr. Build. Mater* 24, 1051–1059. doi:10.1016/j.conbuildmat.2009.11.012

Maslehuddin, M., Allam, I. A., and Ai-Sulainmani, G. J. (1990). Effect of rusting of reinforcing steel on its mechanical properties and bond with concrete. *Mag. J.* 87, 496–502. doi:10.14359/1902

Millington, N., Das, S., and Simonovic, S. P. (2011). The comparison of GEV, log-pearson type 3 and Gumbel distributions in the upper thames river watershed under global climate models. *Water Resour. Res. Rep. no. 077.*

Otieno, M., Beushausen, H., and Alexander, M. (2013). Prediction of corrosion rate in reinforced concrete structures – a critical review and preliminary results. *Mater Corros.* 63, 777–790. doi:10.1002/maco.201106282

Ou, Y. C., Susanto, Y. T. T., and Roh, H. (2016). Tensile behavior of naturally and artificially corroded steel bars. *Constr. Build. Mater* 103, 93–104. doi:10.1016/j.conbuildmat.2015.10.075

Reshvanlou, B. A., Nasserasadi, K., and Ahmadi, J. (2022). An innovative location-dependent stochastic model for prediction steel bars area under chloride ion attack in the presence of transverse rebars. *Constr. Build. Mater* 333, 127390. doi:10.1016/j.conbuildmat.2022.127390

Rosenkrantz, W. A. (2000). Confidence bands for quantile functions: a parametric and graphic alternative for testing goodness of fit. *Am. Statistician* 54 (3), 185–190. doi:10.2307/2685588

Stewart, M. G., and Al-Harthy, A. (2008). Pitting corrosion and structural reliability of corroding RC structures: experimental data and probabilistic analysis. *Reliab Eng. Syst. Saf.* 93, 373–382. doi:10.1016/j.ress.2006.12.013

Stewart, M. G., and Rosowsky, D. V. (1998). Time-dependent reliability of deteriorating reinforced concrete bridge decks. *Struct. Saf.* 20, 91–109. doi:10.1016/s0167-4730(97)00021-0

Tang, F., Lin, Z., Chen, G., and Yi, W. (2014). Three-dimensional corrosion pit measurement and statistical mechanical degradation analysis of deformed steel bars subjected to accelerated corrosion. *Constr. Build. Mater* 70, 104–117. doi:10.1016/j.conbuildmat.2014.08.001

Torres-Acosta, A. A., and Castro-Borges, P. (2013). Corrosion-induced cracking of concrete elements exposed to a natural marine environment for five years. *Corrosion* 69, 1122–1131. doi:10.5006/0844

Xi, X., and Yang, S. (2019). Investigating the spatial development of corrosion of corner-located steel bar in concrete by X-ray computed tomography. *Constr. Build. Mater* 221, 177–189. doi:10.1016/j.conbuildmat.2019.06.023

Xia, J., Jin, W., and Li, L. (2016). Performance of corroded reinforced concrete columns under the action of eccentric loads. *J. Mater Civ. Eng.* 28 (1), 04015087. doi:10.1061/(asce)mt.1943-5533.0001352

Xiao, Q. (2015). A method for calculating quantile function and its further use for data fitting. *arXiv Prepr.* doi:10.48550/arXiv.1508.06125

Yi, W., Kunnath, S. K., Sun, X., Shi, C., and Tang, F. (2010). Fatigue behavior of reinforced concrete beams with corroded steel reinforcement. *ACI Struct. J.* 107, 526–533.

Yuan, Y., Ji, Y., and Shah, S. P. (2007). Comparison of two accelerated corrosion techniques for concrete structures. *ACI Struct. J.* 104, 344–347. doi:10.14359/18624

Zeng, C., Zhu, J. H., Xiong, C., Li, Y., Li, D., and Walraven, J. (2020). Analytical model for the prediction of the tensile behaviour of corroded steel bars. *Constr. Build. Mater* 258, 120290. doi:10.1016/j.conbuildmat.2020.120290

Zhang, J. Z., Huang, J., Fu, C. Q., Huang, L., and Ye, H. L. (2021). Characterization of steel reinforcement corrosion in concrete using 3D laser scanning techniques. *Constr. Build. Mater* 270, 121402. doi:10.1016/j.conbuildmat.2020.121402

Zhang, R., Castel, A., and Francois, R. (2010). Concrete cover cracking with reinforcement corrosion of RC beam during chloride-induced corrosion process. *Cem. Concr. Res.* 40, 415–425. doi:10.1016/j.cemconres.2009.09.026

Zhang, W., Song, X., Gu, X., and Li, S. (2012). Tensile and fatigue behavior of corroded rebars. *Constr. Build. Mater* 34, 409–417. doi:10.1016/j.conbuildmat.2012.02.071

Zhang, W. P., Chen, J. P., Yu, Q. Q., and Gu, X. L. (2021). Corrosion evolution of steel bars in RC structures based on Markov chain modeling. *Struct. Saf.* 88, 102037. doi:10.1016/j.strusafe.2020.102037

Zhang, W. P., Zhou, B. B., Gu, X. L., and Dai, H. C. (2014). Probability distribution model for cross-sectional area of corroded reinforcing steel bars. *J. Mater Civ. Eng.* 26, 822–832. doi:10.1061/(asce)mt.1943-5533.0000888

Zhao, Y., Xu, X., Wang, Y., and Dong, J. (2020). Characteristics of pitting corrosion in an existing reinforced concrete beam exposed to marine environment. *Constr. Build. Mater* 234, 117392. doi:10.1016/j.conbuildmat.2019.117392

Zhu, W., Francois, R., Coronelli, D., and Cleland, D. (2013). Effect of corrosion of reinforcement on the mechanical behaviour of highly corroded RC beams. *Eng. Struct.* 56, 544–554. doi:10.1016/j.engstruct.2013.04.017